Biocatalysis and Agricultural Biotechnology 20 (2019) 101183

Contents lists available at ScienceDirect

Biocatalysis and Agricultural Biotechnology

journal homepage: www.elsevier.com/locate/bab

Biodegradation and detoxification of malachite green by a newly isolated bioluminescent bacterium *Photobacterium leiognathi* strain MS under RSM optimized culture conditions

Shubham S. Sutar[a,1], Prasanna J. Patil[a,1], Asif S. Tamboli[b], Devashree N. Patil[a], Onkar A. Apine[a], Jyoti P. Jadhav[a,*]

[a] Department of Biotechnology, Shivaji University, Vidyanagar, Kolhapur, Maharashtra, 416004, India
[b] Department of Biochemistry, Shivaji University, Vidyanagar, Kolhapur, Maharashtra, 416004, India

ARTICLE INFO

Keywords:
Bioluminescence
Response surface methodology
Malachite green
Biodegradation
Phytotoxicity
Cytotoxicity

ABSTRACT

The isolated bioluminescent bacterium was identified as *Photobacterium leiognathi* strain MS using 16 S rRNA sequence analysis and subjected to malachite green (MG) dye degradation. The Box-Behnken based response surface methodology (RSM) was employed in optimizing medium conditions exhibiting maximum growth at pH 8.0, temperature 30 °C, NaCl 3.5%, and peptone 6.5%. *Photobacterium leiognathi* strain MS was capable of tolerating high concentration of MG (1.0 gL^{-1}) with 92.50% decolorization potency within 24 h. UV-Vis, FTIR, and LC-MS QTOF analyses confirmed biodegradation of MG into several metabolites as well as its catabolism pathway. A significant increase in the activity of laccase was obtained which revealed its major involvement in the degradation of MG dye. Moreover, phytotoxicity and cytotoxicity analyses illustrated that the metabolites generated were less toxic than the parental compound.

1. Introduction

Bioluminescent bacteria are the foremost copious and widely distributed light-emitting organisms. They hold numerous remarkable flamboyant properties, including ability to grow at low temperature (psychrophiles), high salinity (halophiles) and pressure tolerance (barophiles). Malachite green (MG) is a compound belonging to a group of triphenylmethane dyes (Yang et al., 2015), usually used in the textile industries as coloring agents for papers, toys and plastic varieties (Cheriaa and Bakhrouf, 2009). It is also used as a potential agent for treating fungal and protozoal infections in aquaculture and fisheries (Shedbalkar and Jadhav, 2011). In the medical field, it has been utilized as a disinfectant and anthelmintic (Singh and Nakate, 2013). Potential exposure to MG occurs to the people working in dye and aquaculture industries (Culp and Beland, 1996). Its toxicological effects include carcinogenesis, mutagenesis, teratogenesis, chromosomal aberrations, and respiratory toxicity (Srivastava et al., 2004). Hence, it is not approved by the United States Food and Drug Administration and is listed as a priority chemical for carcinogenicity. But, due to its low cost, good efficacy and lack of appropriate alternatives, it is still used in many areas throughout the world.

Previous studies have been reported on different groups of MG decolorizing microorganisms including yeast (Jadhav and Govindwar, 2006), fungi (Jasinska et al., 2012; Shedbalkar and Jadhav, 2011), microalgae (Daneshvar et al., 2007) and bacteria which embrace *Citrobacter sp.* (An et al., 2002), *Mycobacteria sp.* (Jones and Falkinham, 2003), *Aeromonas sp.* (Ren et al., 2006), *Pseudomonas sp.* (Wu et al., 2009), *Achromobacter sp.* (Wang et al., 2011), *Exiguobacterium sp.* (Wang et al., 2012) and *Micrococcus sp.* (Du et al., 2013).

The present study aimed to determine the use of *P. leiognathi* strain MS for the biodegradation and detoxification of MG dye. As per the literature review, the bioluminescent microorganisms and members of genus *Photobacterium* have not yet been reported to degrade and detoxify the MG dye. The experimental data from LC-MS QTOF analysis led us to propose a potential possible pathway for degradation of MG dye.

2. Materials and methods

2.1. Dye and chemicals

Malachite green hydrochloride (Basic green 4), practical grade, CAS

* Corresponding author. Department of Biotechnology, Shivaji University, Kolhapur, 416004, India.
E-mail address: jpjbiochem@gmail.com (J.P. Jadhav).
[1] These authors contributed equally to this work.

https://doi.org/10.1016/j.bcab.2019.101183
Received 3 March 2019; Received in revised form 24 May 2019; Accepted 28 May 2019
Available online 28 May 2019
1878-8181/

No.: 123333-61-9 was purchased from Himedia Co. Ltd. Stock solution of the dye was prepared in distilled water (D/W) and sterilization was performed using 0.22 µm syringe filter (Axiva). All other chemicals were of analytical grade and highest purity.

2.2. Isolation and identification of bioluminescent bacteria, bioluminescence measurements, and acclimatization

A marine fish, saundali (*Lactarius lactarius*) was used as a source to isolate bioluminescent bacteria. For 16S rRNA sequence analysis, DNA sequencing was accomplished from Agile life science technologies, India Pvt. Ltd. Pune. The phylogenetic tree was constructed using MEGA 7 software and the evolutionary history was inferred using the maximum likelihood method. For bioluminescence measurements, the bioluminescence intensities were measured at room temperature using a Varian Cary Eclipse Fluorescence Spectrophotometer (Agilent Technologies, USA, Instrument Serial Number: MY14410002) (Watkins et al., 2018).

To increase the dye decolorizing potency, acclimatization was performed by exposing isolated strain (*P. leiognathi* strain MS) to various MG dye concentrations (Wang et al., 2011). It was performed up to 1.0 gL^{-1} concentration of MG dye. All assays were performed at pH 7.0 and 27 ± 2 °C room temperature under static condition. The acclimatized strain was consistently maintained on dye agar plates and used for further experiments.

2.3. Statistical media optimization by experimental design

Based on the preliminary experiments, variables such as pH, temperature, NaCl, and peptone were identified to have strong effects on the responses. Therefore, these factors were elected as the variables tested in the 29 run experiment of the Box-Behnken design experiment (Table 1). They were designated as A, B, C, and D and boundary conditions for each factor with actual design are depicted in Table 1. These four factors were prescribed into three coded levels, +1, 0, −1 for high, intermediate, and low value, i.e., pH (6, 8 and 10), temperature (25 °C, 30 °C and 35 °C), NaCl (0.5%, 3.5% and 6.5%) and peptone (0.5%, 6.5% and 12.5%).

The relationship between dependent and independent variables was explained by a second order polynomial equation in RSM (Eq.).

$$Y = \alpha_0 + \sum_{i=1}^{n} \alpha_i A_i + \sum_{i=1}^{n} \alpha_{ii} A_i^2 + \sum_{i=1}^{n} \sum_{j=1}^{n} \alpha_{ij} A_i A_j \quad (1)$$

where, Y is the predicted response; α_0 is model intercept; A_i and A_j are independent variables; α_i, α_{ii} and α_{ij} are regression coefficients for linear, square and interaction effects respectively. 'n' indicates the number of independent variables and (n = 4) in this study. All experiments were carried out in triplicate. Bioluminescent bacterial cultures were grown in a shaking condition (120 rpm) and their luminescence output in a.u. (arbitrary unit) and corresponding optical densities (ODs) were estimated after an incubation period of 18 h. Absorbance measurement was performed using a UV-Visible spectrophotometer (UV-1800, Shimadzu, Japan). Design expert software (Version 11.0, Stat-Ease Inc., Minneapolis, USA) was used for statistical analysis and experimental design.

2.4. Decolorization assay

Decolorization of MG was expressed in terms of percentage (%) by few modifications in previously described method (Deng et al., 2008). A UV-Visible spectrophotometer (UV-1800, Shimadzu, Japan) was used for absorbance measurement. Decolorization experiments were performed in triplicate and its activity was calculated as follows:

Table 1
Box-Behnken design matrix with variables along with actual and predicted responses.

Run	Independent variables				Responses					
	Coded variables				OD (Y_1)			Light intensity (Y_2) (a.u.)		
	A:pH	B: Temperature (°C)	C: NaCl (%)	D: Peptone (%)	Actual response	Predicted Response	Externally Studentized Residuals	Actual Response	Predicted Response	Externally Studentized Residuals
1	0	−1	−1	0	0.6020	0.5812	1.205	455.66	445.02	1.643
2	0	0	+1	0	1.24	1.28	−1.524	770.66	775.82	−0.528
3	0	−1	+1	+1	0.5330	0.5428	−0.547	390.32	399.30	−1.345
4	0	0	+1	0	1.22	1.28	−2.617	768.88	775.82	−0.717
5	0	0	+1	0	1.28	1.28	0.063	775.77	775.82	−0.005
6	−1	0	+1	+1	0.5540	0.5370	0.965	401.69	403.62	−0.271
7	0	+1	+1	+1	0.6780	0.6768	0.064	544.56	536.33	1.222
8	+1	0	−1	0	0.4850	0.4810	0.220	355.68	369.01	−2.191
9	+1	0	+1	−1	0.3450	0.3562	−0.625	255.33	250.57	0.681
10	+1	−1	+1	0	0.6350	0.6458	−0.601	511.73	513.30	−0.220
11	+1	0	0	0	0.5890	0.5783	0.594	431.22	429.37	0.261
12	0	0	−1	−1	0.3940	0.3916	0.131	282.33	269.92	1.994
13	0	0	+1	0	1.33	1.28	2.558	783.44	775.82	0.792
14	0	−1	0	0	0.6120	0.6065	0.301	489.55	478.92	1.642
15	−1	+1	+1	0	0.8650	0.8560	0.502	685.55	682.13	0.485
16	0	0	0	−1	0.4800	0.4690	0.616	352.66	355.42	−0.389
17	0	0	0	+1	0.6070	0.6111	−0.227	462.66	473.22	−1.628
18	0	+1	+1	−1	0.5780	0.5722	0.322	419.35	415.09	0.608
19	0	−1	+1	−1	0.4580	0.4632	−0.285	342.55	355.49	−2.105
20	−1	−1	+1	0	0.5550	0.5555	−0.025	404.72	402.53	0.309
21	0	0	−1	+1	0.4210	0.4338	−0.717	321.77	317.17	0.659
22	+1	+1	+1	0	0.5870	0.5883	−0.071	429.99	430.33	−0.047
23	+1	0	+1	+1	0.5300	0.5214	0.478	387.25	378.65	1.283
24	−1	0	−1	0	0.5250	0.5397	−0.827	372.55	379.11	−0.952
25	−1	0	0	0	0.6890	0.6970	−0.443	568.93	560.31	1.287
26	−1	0	+1	−1	0.5150	0.5179	−0.158	360.88	366.65	−0.831
27	0	0	+1	0	1.31	1.28	1.484	780.33	775.82	0.461
28	0	+1	−1	0	0.6010	0.6007	0.016	448.66	456.46	−1.149
29	0	+1	0	0	0.8150	0.8300	−0.849	656.32	664.12	−1.150

$$\% \text{ Decolorization} = \frac{A-B-C}{A} \times 100 \quad (2)$$

A - Initial absorbance
B - Observed absorbance
C - Adsorptive absorbance

2.5. Effect of different physicochemical parameters on decolorization

2.5.1. Effect of dye concentration on decolorization

To analyze the effect of MG concentration on bacterial growth and decolorization process, initial MG concentrations (0.25–1.0 gL^{-1}) were added and kept at optimum pH 7.0 and temperature 30 °C under static condition. Bacterial cells and supernatants were separated after 24 h of incubation via centrifugation at 10000 × *g* for 30 min. The adsorbed residual dye on the biomass was extracted with an equal volume of 1-Butanol (Wu et al., 2009) and centrifuged at 8000 × *g* at 4 °C for 20 min and then both supernatants (culture and 1-Butanol) were used for absorbance measurement (λ_{max} = 618 nm). Bacterial cell count was estimated by centrifugation at 7000 × *g* at 4 °C for 20 min. The obtained cell pellet washed with sterile NS (Normal saline, 0.85%) until the complete removal of dye. An equal volume of sterile NS was added and absorbance was measured at 600 nm. McFarland standard absorbance values were used to calculate bacterial cell count.

2.5.2. Effect of shaking, static as well as aerobic and anaerobic conditions on MG decolorization

The impact of shaking and static conditions on MG decolorization was analyzed at optimum pH and temperature with shaking at 100 rpm and at static condition. Impact of aerobic as well as anaerobic conditions on decolorization was conjointly studied using Mineral oil overlay technique. Both the experiments were performed at the concentration of 100 μg ml^{-1}.

2.6. Product characterization

2.6.1. FTIR analysis

For FTIR analysis, the culture broth after MG decolorization was centrifuged at 10000 × *g* at 4 °C for 30 min. The supernatant obtained was mixed with an equal volume of ethyl acetate and kept it for 24 h with intermediate shaking in separating funnel. The solvent extract was then dried by evaporation. FTIR analysis was done in the mid-IR region of 4000–400 cm^{-1} with 16 scan speed and samples were recorded using an FT/IR-4600 type A spectrometer, JASCO, Tokyo, Japan.

2.6.2. LC-MS QTOF analysis

2.6.2.1. Sample preparation. After every 2 h, the sample was harvested via centrifugation. The supernatant was extracted using ethyl acetate (1:1), followed by the concentration of extract by rotary evaporation (Superfit continental Pvt. Ltd., Model: PBV-7). Further dried sample was reconstituted with mobile phase and sample was injected to mass spectrometer. Details of the instrument parameters were mentioned as follows:

For LC-MS QTOF analysis, the dried extract of the solvent was dissolved in the mobile phase. The sample 5 μl was injected into an HPLC system (Agilent 1290 binary high pressure, equipped with a ZORBAX RRHD Eclipse plus C-18 analytical column of 3.0 × 100 mm, 1.8 μm particle size) coupled with Agilent 6540 UHD Accurate-Mass Q-TOF LC-MS. The compounds were resolved by using solvent A: 0.1% Formic acid and solvent B: Acetonitrile with 0.1% Formic acid. The flow rate was kept at 0.2 ml min^{-1}. A linear gradient was set as: t = 0–1, A = 75%; t = 1–3, A = 55%; t = 3–7, A = 5%; t = 7–10, A = 95%. The column effluent was introduced into the Dual AJS electrospray ionization source of the mass spectrometer in positive ion mode. The MS parameters were set as: capillary voltage 4.5 kV; nebulizer pressure 30 psi; drying gas flow 11 L min^{-1}; drying gas temperature 350 °C; fragmentor voltage 165 V. LC-MS QTOF accurate mass spectra were recorded across the range 50–1000 *m/z*. Data processing was carried out with Mass Hunter Workstation Qualitative software (version B.06.00, USA). The reference masses were 121.05 *m/z* and 922.00 *m/z*.

2.7. Preparation of cell-free extracts

After decolorization, the sample was centrifuged at 8000 × *g* at 4 °C for 20 min. The supernatants were used as extracellular enzymes. The cell pellets were suspended in 50 mM sodium phosphate buffer (pH 7.0) and sonicated (sonics-vibracell ultrasonic processor) at 4 °C, each of 60 amplitude for 30 s with 2 min time interval. The sonicated cells were centrifuged at 8000 × *g* at 4 °C for 20 min. The supernatants (extracellular and intracellular) obtained were filtered through 0.22 μm membrane filter (Axiva), and used as the source of enzymes.

2.8. Enzyme assays

Several oxidative enzymes have been stated to aid in dye decolorization in bacteria in recent times (Du et al., 2013). In the present study, the four different enzymes, viz., laccase, veratryl alcohol oxidase, tyrosinase and DCIP reductase were scrutinized to identify whether these enzymes are involved in the decolorization of MG. The enzyme assays were conducted with the slight modification from previous methods (Jadhav and Govindwar, 2006; Du et al., 2011; Lade et al., 2015). The activities of these four enzymes were assayed spectrophotometrically. The activity of laccase was determined for different substrates, viz., toluidine, ABTS (2, 2′-azino-bis-3-ethylbenzothiazoline-6-sulfonic acid), and syringaldazine. For toluidine (λ_{max} = 366 nm) and ABTS (λ_{max} = 420 nm), laccase activity was determined in a reaction mixture of 2 ml containing 1.5 ml of 0.1 M acetate buffer (pH 4.8), 0.2 ml enzyme and 0.3 ml respective substrates, 10% ABTS and 0.15% toluidine. For syringaldazine (λ_{max} = 530 nm), 2 ml of the reaction mixture was prepared by adding 1.5 ml of 0.1 M acetate buffer (pH 4.2), 0.2 ml enzyme and 0.3 ml 0.28 mM syringaldazine. The activity of tyrosinase (λ_{max} = 475 nm) was determined in a reaction mixture containing 1.4 ml of 50 mM potassium phosphate buffer (pH 6.0), 0.1 ml enzyme, and 0.5 ml 2 mM L-DOPA (3, 4-dihydroxyphenylalanine). For NADH-DCIP reductase (λ_{max} = 475 nm) activity, the assay mixture contained 50 μM DCIP, 28.57 mM NADH in 50 mM potassium phosphate buffer (pH 7.4) and 0.1 ml enzyme solution (sonicated cells suspension) in a total volume of 5.0 ml. Veratryl alcohol oxidase (λ_{max} = 310 nm) activity was determined using veratryl alcohol as a substrate. Reaction mixture (2 ml) contained 4 mM veratryl alcohol in 1.7 ml 50 mM citrate phosphate buffer (pH 3) and 0.2 ml enzyme to start the reaction. Total protein content was determined by Lowry method, using bovine serum albumin as a standard. All the assays were performed in triplicate.

2.9. Toxicity studies

2.9.1. Phytotoxicity study

Vigna radiata and *Lens culinaris* seeds were used to evaluate the toxicity of MG and its degraded solution. 10 seeds were germinated in petri plate having wetted cotton with 0.1 gL^{-1} MG dye and its degraded solution of the identical concentration in the respective plates. Seeds germinated in water wetted petri plates were used as a control. The phytotoxicity study was performed at room temperature for 3 days and watered with the same solution as per experimental setup. All experiments were performed in triplicate. Percentage of seed germination (% G), Seedling vigor index (SVI) and Root length stress tolerance index (RLSTI) were calculated as per the methods mentioned by Amin et al. (2013).

2.9.2. Cytotoxicity study

In the present study, the cell toxicity of MG and its degraded solution was studied using *Allium cepa*. The bulbs were placed in the

solution of MG, MG degraded solution (concentration 100 μg ml^{-1}) and in water as a control for 4 days at room temperature. Test solutions were reinstated every day throughout the experiment. At the 5th day the length of roots of each bulb was measured. Staining procedure for root tips was carried out as per protocol specified by Chukwujekwu and Van Staden (2014) with some modifications. Finally, interphase and dividing cell counts were studied. The Mitotic index (%), No. of aberrant cells (%) and Percent Root length were calculated as per mentioned by Akinboro and Bakare (2007).

3. Results and discussion

3.1. Isolation and identification of bioluminescent bacteria

A bacterial strain capable of showing bioluminescence was successfully isolated (Fig. S1) and identified as *P. leiognathi* strain MS by 16S rRNA gene sequence analysis. The sequence was deposited in the GenBank database under accession no. KY672852. Phylogenetic position of *P. leiognathi* strain MS is shown in Fig. S2.

3.2. Media optimization, model building and statistical analysis by RSM

3.2.1. Experimental design

A 29-run Box-Behnken, fitting a second-order response surface is tabulated in Table 1 along with actual and predicted responses.

3.2.2. Response surface analysis of optical density (OD)

The data obtained from the experimental runs were subjected to multiple regression analysis. The obtained coefficients were used to build the following equation:

$$OD = + 1.28 - 0.0443 \times A + 0.0607 \times B + 0.0637 \times C + 0.0461 \times D - 0.0895 \times A \times B - 0.0150 \times A \times C + 0.0365 \times A \times D + 0.0510 \times B \times C + 0.0063 \times B \times D + 0.0250 \times C \times D - 0.3473 \times A^2 - 0.2667 \times B^2 - 0.3541 \times C^2 - 0.4450 \times D^2 \quad (3)$$

Maximum OD (1.328) was observed at pH 8.0, temperature 30 °C, NaCl 3.5% and peptone 6.5%. As shown in Table 2, ANOVA of regression model demonstrated that the model was highly significant, as it was evident from the fisher's 'F' test with a very low probability value (p-value of model ≤ 0.0001), with high F-value (230.98). Linear effects of pH, temperature, NaCl, peptone, interaction effects of pH with temperature (AB), pH with peptone (AD) and temperature with NaCl (BC), square effects of all four factors, viz., pH (A^2), temperature (B^2), NaCl (C^2) and peptone (D^2) respectively, were found significant terms for OD. The F-value of 0.11 implies the lack of fit was not significant and the predicted R^2 of 0.9893 was in reasonable agreement with the adjusted R^2 of 0.9914; indicated that this response surface design can be used for modeling the design space. In our study, signal to noise ratio (adequate precision) was observed to be 47.0482. As the value of 47.0482 implies adequate signal, this model can be used to navigate the design.

Table 2
ANOVA statistics for the fitted quadratic polynomial of OD.

Source	Sum of squares	df	Mean square	F-value	p-value	
Model	2.39	14	0.1705	230.98	< 0.0001	significant
A-pH	0.0236	1	0.0236	31.96	< 0.0001	
B-Temperature	0.0443	1	0.0443	60.01	< 0.0001	
C–NaCl	0.0486	1	0.0486	65.91	< 0.0001	
D-Peptone	0.0255	1	0.0255	34.53	< 0.0001	
AB	0.0320	1	0.0320	43.42	< 0.0001	
AC	0.0009	1	0.0009	1.22	0.2881	
AD	0.0053	1	0.0053	7.22	0.0177	
BC	0.0104	1	0.0104	14.10	0.0021	
BD	0.0002	1	0.0002	0.2117	0.6525	
CD	0.0025	1	0.0025	3.39	0.0870	
A^2	0.7825	1	0.7825	1060.35	< 0.0001	
B^2	0.4614	1	0.4614	625.20	< 0.0001	
C^2	0.8132	1	0.8132	1101.96	< 0.0001	
D^2	1.28	1	1.28	1740.20	< 0.0001	
Residual	0.0103	14	0.0007			
Lack of Fit	0.0023	10	0.0002	0.1120	0.9975	not significant
Pure Error	0.0081	4	0.0020			
Cor Total	2.40	28				

3.2.3. Response surface analysis of light intensity

The second order polynomial model for light intensity was regressed by only the significant terms represented in equation obtained by using regression coefficients as shown below:

$$\text{Light Intensity} = + 775.82 - 35.26 \times A + 49.16 \times B + 60.39 \times C + 41.26 \times D - 90.64 \times A \times B - 30.21 \times A \times C + 22.78 \times A \times D + 43.44 \times B \times C + 19.36 \times B \times D + 17.64 \times C \times D - 172.72 \times A^2 - 96.04 \times B^2 - 168.66 \times C^2 - 253.23 \times D^2 \quad (4)$$

The results of ANOVA analysis (Table 3) showed that this model was highly significant ($p \leq 0.01$) with F- value of 474.21. The predicted R^2 of 0.9887 was in reasonable agreement with the adjusted R^2 of 0.9958. However, Non-significant lack of fit was good. In the present model, the lack of fit F-value was 3.73 implies the lack of fit was not significant relative to the pure error and can be used for further analysis. Hence, this analysis permitted the use of response surface for modeling the design space. Notably, all factors have exerted a significant effect on light intensity as all of them possess p - value ≤ 0.05. The adequate precision was observed to be 68.737 indicating an adequate signal implies requisite quadratic model.

In this study, maximum bioluminescence was observed (783.448 a.u.) at pH 8.0, temperature 30 °C, NaCl 3.5% and peptone 6.5%. Here, we observed a direct relationship between OD and luminescence as OD increased, luminescence was also increased and vice versa.

3.2.4. Effect of different variables on OD and light intensity

3D surface plots and contour plots were used to study the interaction effects of two variables AB, AC, AD, BD, BC, and CD on optical density and light intensity. As we can observe in Fig. 1a and g, bacterial growth was significantly affected by the lower and higher concentrations of pH and temperature. The elliptical shape of a contour plot showed a highly significant interaction between pH and temperature. In the present study, there was less bacterial growth observed as we moved towards more alkaline or acidic pH. In case of temperature, very low (below 10 °C) and very high (above 40 °C) levels were predominantly affected the bacterial growth. There was no growth observed below very low and beyond very high temperature. Hence, there was no bioluminescence observed. The maximum OD (1.328) and light intensity (783.448 a.u.) were observed at optimum pH (8.0) and temperature (30 °C). Fig. 1b and h, demonstrate the interactive effect of pH and NaCl on OD and light intensity which showed quadratic response. Effect of NaCl on OD and light intensity was less effective at lower pH than the higher. This could be attributed to the fact that pH optima was in the range of 7.0–8.5. Hence, the response was lower above and below this range. OD and light intensity were increased with increase in NaCl concentration and vice-versa. In present study, the maximum concentration tolerated by bacteria was 7.5% and beyond this no growth was observed. Among all factors, NaCl showed a marked effect on cell density and light intensity probably due to halophilic nature of *P. leiognathi* strain MS. The circular nature of the contour plot of OD showed a moderate interaction between NaCl and pH, while elliptical nature of contour plot showed the interaction was highly significant in case of light intensity. In the previous report, the optimum concentration of NaCl identified was 3.1% (Lee et al., 2001). However, the maximum values of OD and bioluminescence were observed at NaCl 3.5% (optimum). As evident from Fig. 1c and i, pH and peptone had

Table 3
ANOVA statistics for the fitted quadratic polynomial of light intensity.

Source	Sum of squares	df	Mean square	F-value	p-value	
Model	749500	14	53533.26	474.21	< 0.0001	significant
A-pH	14919.07	1	14919.07	132.16	< 0.0001	
B-Temperature	28999.09	1	28999.09	256.88	< 0.0001	
C–NaCl	43763.79	1	43763.79	387.67	< 0.0001	
D-Peptone	20431.04	1	20431.04	180.98	< 0.0001	
AB	32864.07	1	32864.07	291.12	< 0.0001	
AC	3650.46	1	3650.46	32.34	< 0.0001	
AD	2075.21	1	2075.21	18.38	0.0008	
BC	7548.05	1	7548.05	66.86	< 0.0001	
BD	1499.32	1	1499.32	13.28	0.0027	
CD	1244.47	1	1244.47	11.02	0.0051	
A^2	193500	1	193500	1714.02	< 0.0001	
B^2	59823.44	1	59823.44	529.93	< 0.0001	
C^2	184500	1	184500	1634.40	< 0.0001	
D^2	416000	1	416000	3684.70	< 0.0001	
Residual	1580.46	14	112.89			
Lack of Fit	1427.25	10	142.72	3.73	0.1083	not significant
Pure Error	153.21	4	38.30			
Cor Total	751000	28				

significant interactions for OD and light intensity. The maximum concentration of peptone used in the present study was 12.5% above which less growth was observed while the optimum concentration was 6.5%.

The effect of interaction between temperature and NaCl on OD and light intensity is depicted in Fig. 1d and j, indicates a significant interaction between them and it moderately affected the response. In addition, the OD and light intensity were hampered by their higher and lower levels. The response surface curves showed in Fig. 1e and k, illustrated that the interaction between temperature and peptone was highly significant for light intensity and it possesses the elliptical contour plots, while, it was insignificant for OD. Fig. 1f and l showed the interactive effect of NaCl and peptone on OD and light intensity, which found to be insignificant for OD, while it was significant for light intensity. It was found that increased or decreased concentration of peptone didn't affect the effectiveness of both on OD and light intensity.

In this study, we have accomplished medium optimization of this bacterium, in order to obtain a maximum surface area for the maximum growth so as to induce higher decolorization potency. As this bacterium is a strict halophile, we obtained profoundly efficient growth of this bacterium in the regular water body. In our experiment, we exposed our bacterium to Nutrient Broth [(NB) having a composition (gL^{-1}), 10.0 Peptone, 10.0 Beef extract, 5.0 NaCl, pH 7.3 ± 0.1], to investigate its decolorization potency. We obtained maximum decolorization 82% at 1 gL^{-1} concentration, in comparison with 92.5% at 1 gL^{-1} MG dye in LM medium. Thus, this result indicated that this bacterium has a novel ability to endure high stress environments like high salinity, as well as low salinity (real water bodies). Hence, this bacterium is a paramount choice for the bioremediation of textile effluent not only in coastal areas but also in local water bodies.

3.3. Effect of different physicochemical parameters on decolorization

3.3.1. Effect of dye concentration on MG decolorization

Fig. 2C showed the influence of initial MG concentration on decolorization and cell biomass. The amount of % decolorization varied with varying initial dye concentration. An inverse relationship between MG concentration and decolorization was observed. The results indicated that decolorization potency decreased from 98.23 to 92.50% as the initial dye concentration increased from 0.25 to 1.0 gL^{-1}. These results intimated that an increase in dye concentration might be affecting the enzyme activity concerned in decolorization and degradation of MG, ultimately resulting in the decreased decolorization rate. Similar results were observed in the studies carried out by Kagalkar et al. (2011) and Ayed et al. (2009). On the other hand, as initial dye concentration increased (0.25–1.0 gL^{-1}), cell biomass concentration in terms of colony forming units ml^{-1} was also increased (10.80×10^8 to 27.93×10^8 CFU ml^{-1}), intimating that MG or its degraded products might be utilized by bacteria for their growth.

3.3.2. Effect of shaking, static as well as aerobic and anaerobic conditions on MG decolorization

Higher decolorization % was observed in the static condition (92.80%) as compared to the shaking condition (89.17%). As these bacteria grow well in shaking condition, simply increased bacterial count was observed (19.03×10^8 and 12.33×10^8 CFU ml^{-1} for shaking and static respectively) as shown in Fig. 2B. The results obtained prompted that decolorization was independent on the concentration of aerobic molecular oxygen. Decolorization was achieved in both aerobic and anaerobic (static) conditions (Fig. 2B). In aerobic, it was achieved at a higher percentage (92.04%) while less in anaerobic condition (83.73%). Bacterial cell count (CFU ml^{-1}) was observed to be same in both the aerobic and anaerobic conditions (11.47×10^8 and 11.57×10^8 CFU ml^{-1}) respectively.

3.4. Product characterization

3.4.1. FTIR analysis

In order to confirm the degradation of malachite green by *P. leiognathi* strain MS, the dye solution was subjected to FTIR spectral analysis, before and after degradation. The results obtained showed noteworthy variation in the fingerprint region (1500-500 cm^{-1}) of FTIR spectra of MG and MG degraded solution. For the MG, peaks in the fingerprint region (1500-500 cm^{-1}) correspond to the mono-substituted and para-substituted benzene rings, supporting peaks to this were observed at 1635.34 cm^{-1} for C=C stretching vibration of the mono-substituted and para-substituted benzene rings. A peak at 1218.79 cm^{-1} for C–N stretching vibrations represent the presence of amino groups and a peak at 770.42 cm^{-1} for C–H bending vibrations represents the presence of methylene groups. Spectrum conjointly showed peaks at 3313.11 cm^{-1} for O–H stretching vibrations for secondary amines. Moreover, the absence of all these peaks in the spectrum of MG degraded solution strongly indicated that *P. leiognathi* strain MS mediated biotransformation of MG resulted in degradation of MG. The fingerprint region of MG degraded solution revealed the emergence of new peaks (1435.74 and 1404.85 for OH, 951.78 and 666.29 for C=C, 2995.87 and 2911.02 for C–H, 3433.64 for N–H). Therefore, the present results of FTIR analysis intimate that the prominent exposed functional groups in the MG degraded solution include –OH, N–H,

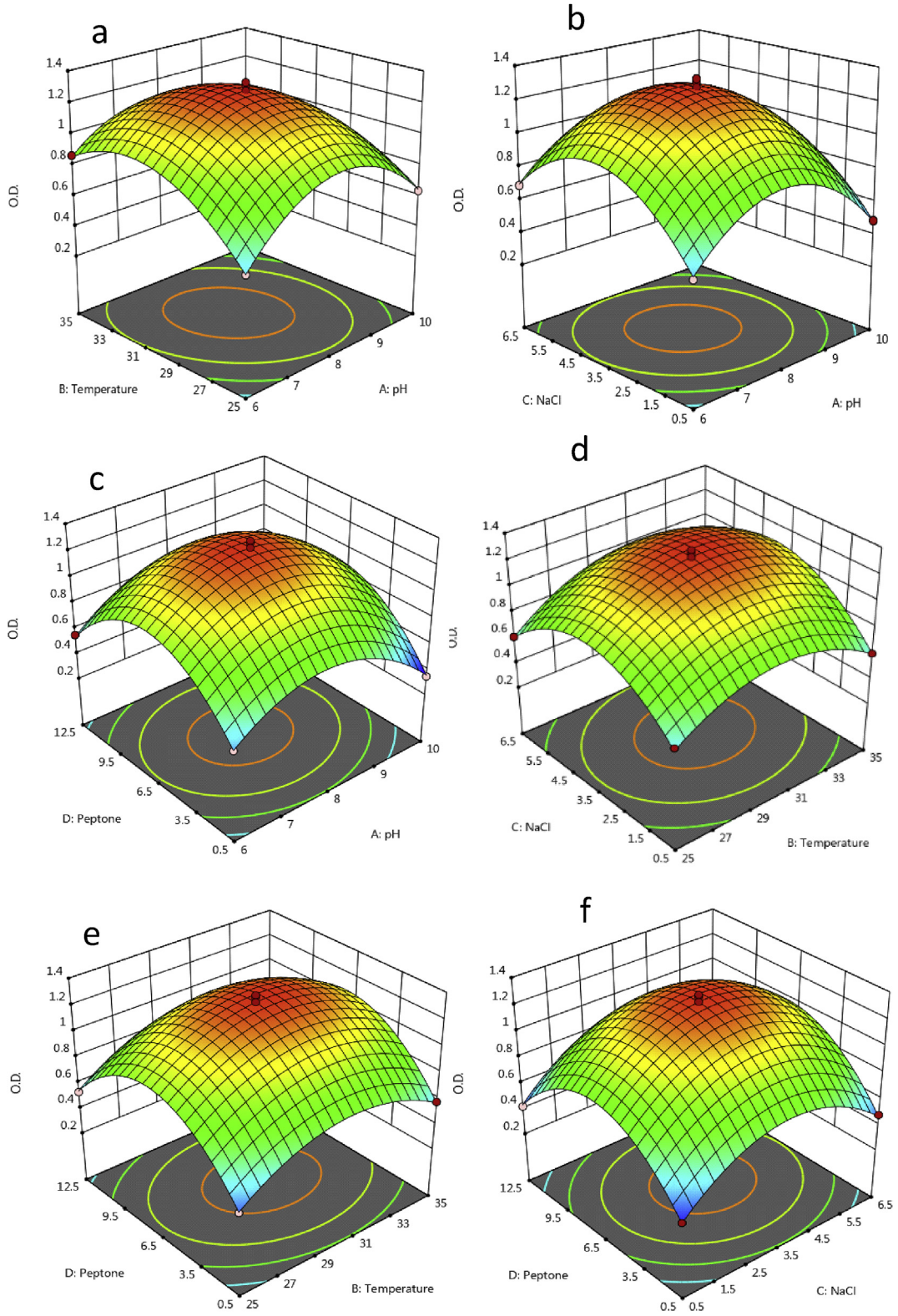

Fig. 1. Three-dimensional response surface curves of OD (a) pH and temperature; (b) pH and NaCl; (c) pH and peptone; (d) temperature and NaCl; (e) temperature and peptone; (f) NaCl and peptone, and light intensity (g) pH and temperature; (h) pH and NaCl; (i) pH and peptone; (j) temperature and NaCl; (k) temperature and peptone; (l) NaCl and peptone.

C═C, C–H, which corroborates the MG degradation.

3.4.2. LC-MS QTOF analysis

UV-Visible spectra of MG degraded solution showed the disappearance of the most important peak of MG at 618 nm and two minor peaks at 315 nm and 425 nm respectively (Fig. 2A).

The current study involved extraction of samples at different time intervals followed by LC-QTOF MS-MS analysis. Target m/z values were selected based on previous reports available on MG degradation and initial screening through LC-MS QTOF. Results showed that the

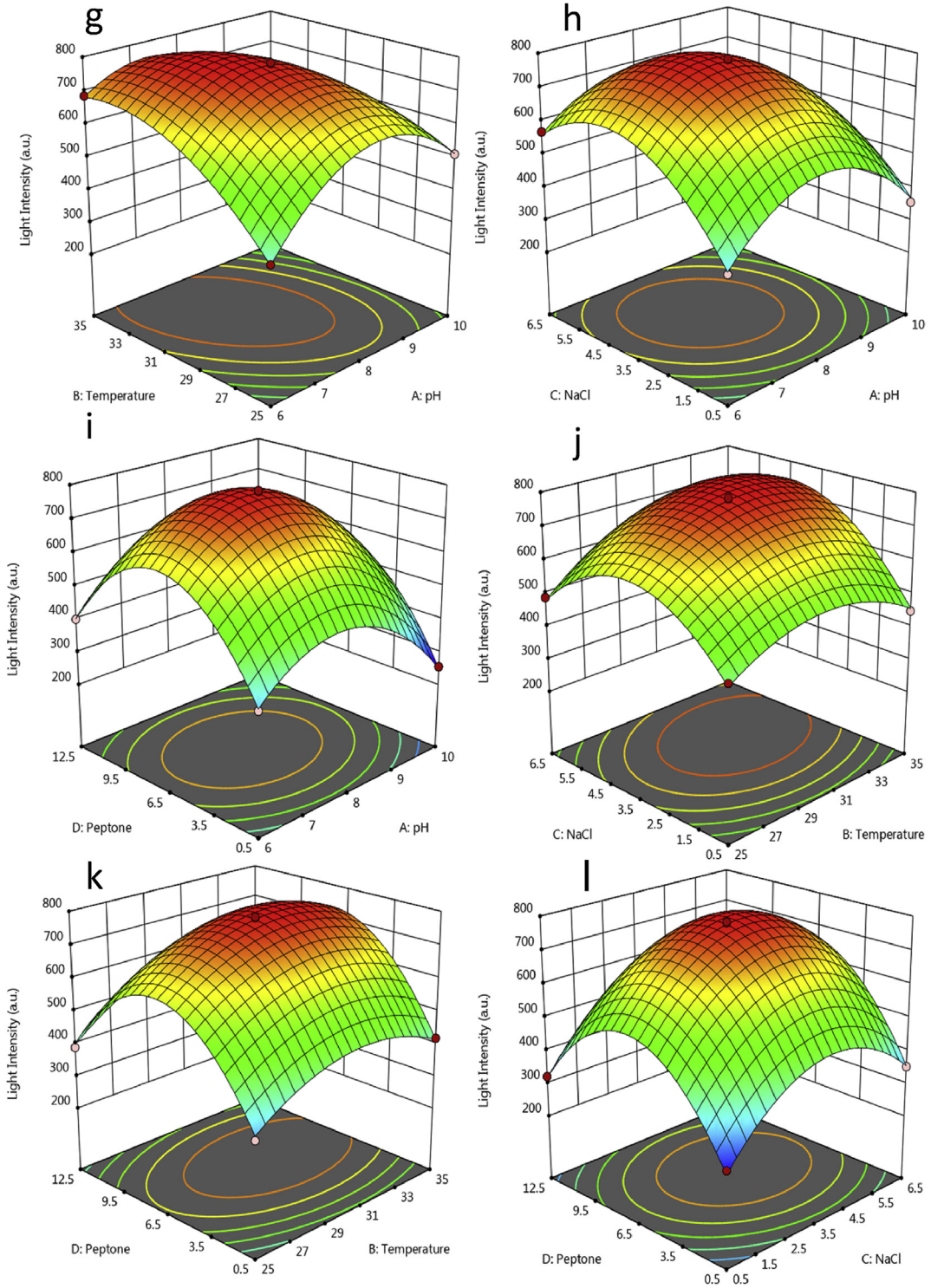

Fig. 1. (*continued*)

degradation of MG by *P. leiognathi* strain MS showed the presence of two different pathways. The simultaneous presence of both pathways eventually results in rapid and efficient degradation of MG as indicated in Fig. 3. Pathway I concerned sequent demethylation of MG forming desmethyl derivatives of MG i.e. mono, di, tri, and tetradesmethyl MG which was similar to Yang et al. (2015) and Lee and Kim (2012). It is vital to note that decolorization of MG is not due to N-demethylation of MG i.e. formation of mono, di, tri, and tetradesmethyl MG but further degradation of MG must occur to destruct the chromophore structure (Yang et al., 2015). Generally, central carbon radical formation due to hydroxylation destructs the dye chromophore structure (Chen et al., 2007; Oturan et al., 2008). Pathway II involved hydroxyl radical attack on MG at central carbon position producing pseudo base or carbinol form of MG. This form of MG was found to be colorless, therefore the transformation of MG into carbinol form initiated decolorization process. This carbinol form of MG further broken down at the bond between the central carbon atom and N, N-dimethyl amino phenyl rings by oxidation, resulting in the formation of (dimethyl amino-phenyl)-phenyl methanone and N, N-dimethyl aniline. (Dimethyl amino-phenyl)-Phenyl methanone further sequentially demethylated to form

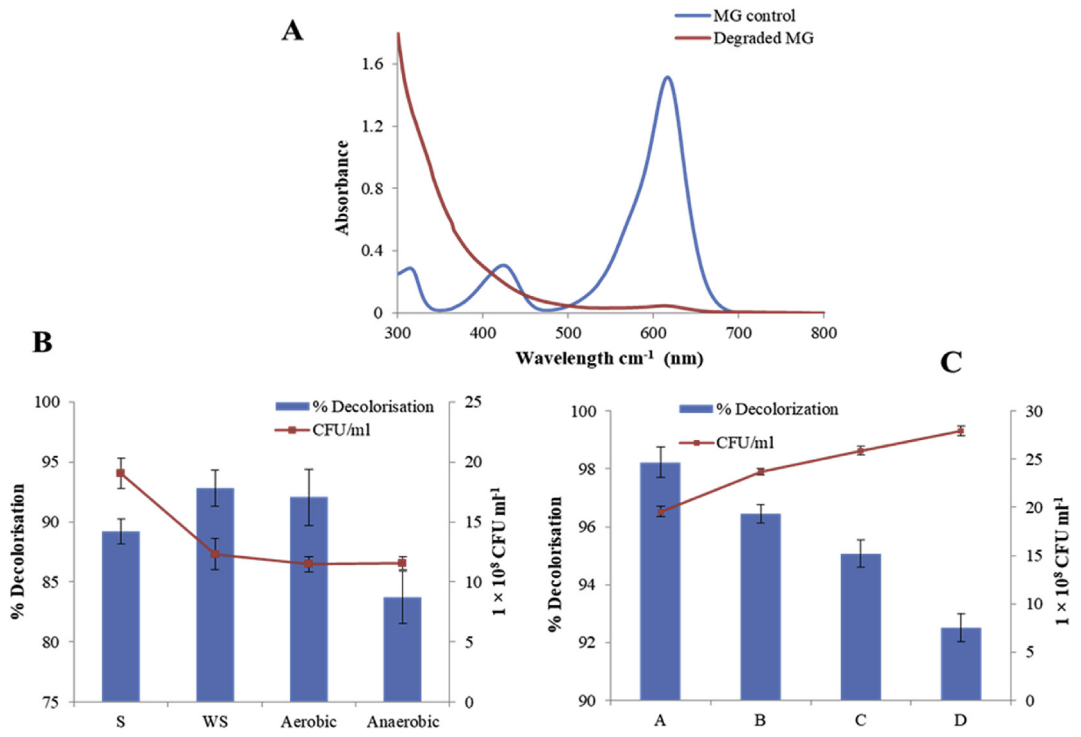

Fig. 2. (A) UV-Visible spectra of before (MG) and after (MG D) treatment with *P. leiognathi* strain MS at a concentration of 100 μg ml^{-1}, at pH 7.0, temperature 30 °C, under static condition (B) Effects of shaking (S), static (WS), aerobic, and anaerobic conditions on MG decolorization efficiency by *P. leiognathi* strain MS, at pH 7.0, and temperature 30 °C. Each point represents mean ± SD. (C) Effect of initial MG concentration (gL^{-1}) A. 0.25, B. 0.5, C. 0.75, D. 1.0, at pH 7.0, temperature 30 °C, under static condition.

(methyl amino-phenyl)-phenyl methanone and (aminophenyl)-phenyl methanone. Besides pathway I and II, in addition (dimethyl amino-phenyl)-phenyl methanone oxidized to produce 4-dimethyl benzoic acid and benzene, (methyl amino-phenyl)-phenyl methanone, oxidized to form 4-methyl benzoic acid and benzene and finally (aminophenyl)-phenyl methanone oxidized to form aminobenzoic acid and benzene resulted in the complete degradation of MG as shown in Fig. 3.

It was obvious that as the aromatic ring opened, the formation of different types of compounds was expected. The proposed degradation pathway relied upon the 14 compounds identified by LC-MS QTOF analysis. The mass spectra of MG and its degraded metabolites are given in Fig. S4 to support the biodegradation pathway. Several previous studies on MG degradation involved the formation of a leuco form of MG (LMG), which is highly toxic reduced form of MG (Cha et al., 2001; Wang et al., 2011; Jasinska et al., 2012). In our study of *P. leiognathi* strain MS mediated MG degradation, the reduced form LMG was not detected.

3.5. Enzyme assays

In the present study, the highest enzyme activity was observed in extracellular crude extract of enzymes with preference to substrate toluidine 0.417 ± 0.008 U mg of protein^{-1} min^{-1}, while for ABTS 0.136 ± 0.004 U mg of protein^{-1} min^{-1} and 0.143 ± 0.003 U mg of protein^{-1} min^{-1} for syringaldazine. The intracellular crude extract of the enzyme also showed the laccase enzyme activity, for toluidine it was 0.154 ± 0.002 U mg of protein^{-1} min^{-1}, while 0.115 ± 0.017 U mg of protein^{-1} min^{-1} for ABTS and 0.097 ± 0.004 U mg of protein^{-1} min^{-1} for syringaldazine. In addition, tyrosinase enzyme activity was also calculated, for intracellular it was observed to be 0.016 ± 0.001 U mg of protein^{-1} min^{-1} and for extracellular it was 0.240 ± 0.002 U mg of protein^{-1} min^{-1}. For NADH-DCIP reductase, the intracellular activity found was 0.265 ± 0.003 U mg of protein^{-1} min^{-1} and extracellular activity was 0.397 ± 0.002 U mg of protein^{-1} min^{-1}. Moreover, intracellular and extracellular activities for Veratryl alcohol oxidase were 0.042 ± 0.003 U mg of protein^{-1} min^{-1} and 0.074 ± 0.001 U mg of protein^{-1} min^{-1} respectively. The ability of extracellular and intracellular crude extracts of the enzyme to oxidize different common substrates especially toluidine suggested that the induction of laccase enzyme activity during the degradation of MG by *P. leiognathi* strain MS.

In our study, the effect of MG on the induction of polyphenol oxidases (laccase and tyrosinase) and oxidoreductases (NADH-DCIP reductase and Veratryl alcohol oxidase) was also assessed to scrutinize percentage variation in their activities. It was found that 49.46% (extracellular) and 53.12% (intracellular) enzyme activity of laccase was induced by the addition of MG. Similarly, induction of tyrosinase by addition of MG was found to be 17.05% and 2.32% for extracellular and intracellular respectively. In case of oxidoreductases, NADH-DCIP reductase had 28.21% (extracellular) and 38.46% (intracellular) induction in the enzyme activity. While, for veratryl alcohol oxidase, the percentage induction in the enzyme activity was 5.25% and 6.09% respectively for both extracellular as well as intracellular. Thus, significant increase in the activities of these enzymes indicated involvement of these enzymes for MG degradation. Based on the obtained results, it was found that the laccase was more active and favored the initial breakdown of MG followed by the induction of other enzymes. Mutual action of these oxidoreductases as well as polyphenol oxidases was responsible for biodegradation and detoxification of MG.

3.6. Toxicity studies

3.6.1. Phytotoxicity study

The values of %G, SVI, RLSTI of control, MG and MG degraded solution intimated that MG was toxic to both *Vigna radiata* and *Lens culinaris* seeds. There was 60% and 70% inhibition of seed germination observed in MG solution treated with *Vigna radiata* and *Lens culinaris* seeds respectively as shown in Table 4. The extracted metabolites or

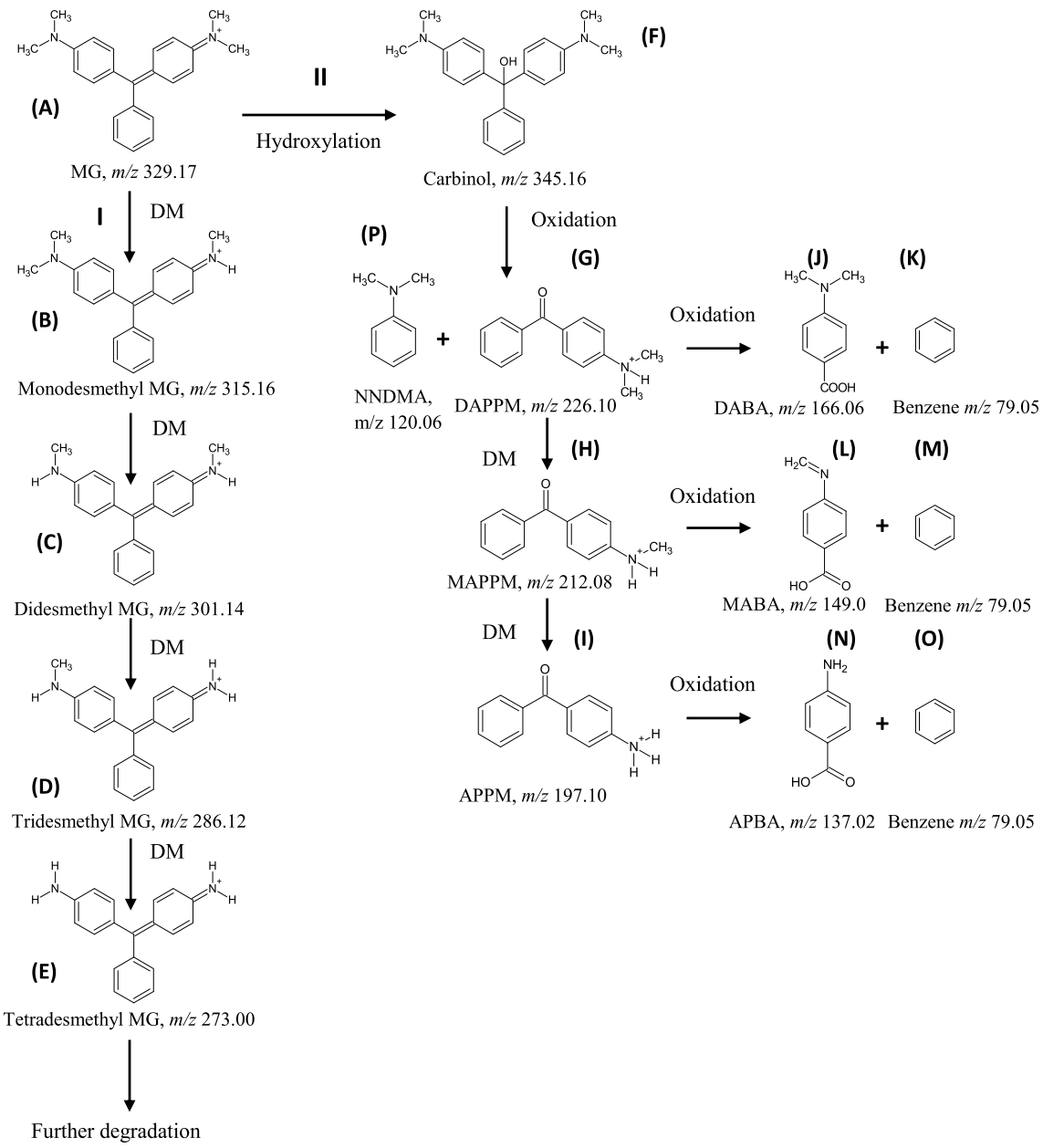

Fig. 3. Proposed mechanism of MG degradation in *P. leiognathi* strain MS.(A) MG, (B) Monodesmethyl MG, (C) Didesmethyl MG, (D) Tridesmethyl MG, (E) Tetradesmethyl MG, (F) Carbinol (G) (Dimethyl amino-phenyl)-phenyl-methanone (DAPPM), (H) (methyl amino-phenyl)-phenyl-methanone (MAPPM), (I) (amino phenyl)-phenyl methanone (APPM), (K), (M), (O) Benzene, (J) 4-Dimethyl amino benzoic acid (DABA), (L) Methyl amino benzoic acid (MABA), (N) Amino phenyl benzoic acid (APBA), (P) N, N-Dimethyl aniline (NNDMA). (I. II. stands for pathway I. and II. respectively and DM for Desmethyl MG).

Table 4
Phytotoxicity comparison study of MG and its degraded solution on Vigna radiata and Lens culinaris.

	Water	*Vigna radiata*			*Lens culinaris*	
		MG degraded solution	MG solution	Water	MG degraded solution	MG solution
% G	100	100	45 ± 5.0**	100	100	35 ± 5.0**
Root length (cm)	4.04 ± 0.15	2.83 ± 0.27*	0.67 ± 0.12**	2.12 ± 0.07	1.54 ± 0.07*	0.17 ± 0.02***
Root length (%)	100	69.80 ± 4.0**	16.47 ± 2.33***	100	72.66 ± 0.96***	8.20 ± 0.89***
SVI	404.5 ± 15.50	283.0 ± 27.0*	30.75 ± 8.75**	212.5 ± 7.50	154.5 ± 7.50*	6.25 ± 1.75***
RLSTI	0.0	67.88 ± 2.08***	15.35 ± 1.21**	0.0	72.68 ± 0.96***	8.20 ± 0.88**

The values are mean of two experiments ± SEM. significantly different from control at *$p \leq 0.05$, **$p \leq 0.01$, ***$p \leq 0.001$ by one-way analysis of variance (ANOVA) with Tukey-Kramer comparison test.

Table 5
Cytological effects of treatment with MG and its degraded solution on A. cepa root tip cells.

	Germination	No. of cells examined	No. of dividing cells	Mitotic index (%)	Aberrant cells (%)
Control	Yes	500	262.50 ± 7.50	52.50 ± 1.50	0
MG D	Yes	500	226.0 ± 6.0*	45.20 ± 1.20*	4.0 ± 1.0**
MG	No	–	–	–	–

The values are mean of two experiments ± SEM. significantly different from control at *$p \leq 0.05$, **$p \leq 0.01$. ***$p \leq 0.001$ by one-way analysis of variance (ANOVA) with Tukey-Kramer comparison test.

MG degraded solution was observed to be far less toxic than MG. Hence *P. leiognathi* strain MS mediated biotransformation of MG into metabolites resulted in detoxification of MG. As compared to control, in MG degraded solution seedling root length observed to be less, intimating that MG degraded solution was more sensitive to seedling root elongation. Similar results were observed in the previous reports of Yang et al. (2015); Shedbalkar and Jadhav (2011).

3.6.2. Cytotoxicity study

The results of the effect of MG, MG degraded solution on root growth of *A. cepa* are shown in Table 5. There was no germination of bulbs observed in MG solution intimating that MG was highly toxic to *Allium cepa*. The values obtained from % RL, % MI and % aberrant cells showed decreased root elongation in MG degraded solution as compared to control. Earlier reports suggested that whenever there was a decrease in root elongation there was always a reduction in no. of dividing cells. In the present study, MI of bulbs kept in MG degraded solution was observed to be slightly decreased as compared to control and few chromosomal aberrations were also observed. As per Timothy et al. (2014), declination in MI attributed to the interference in the cell cycle and increased incidences of chromosomal aberrations were observed. In the present study, majorly anaphase bridges were observed (Fig. S5 i). Overall results suggested that MG was extremely toxic to roots of *A. cepa*. The metabolites or MG degraded solution obtained from *P. leiognathi* mediated biotransformation was far less toxic than the MG dye.

4. Conclusion

The current study elucidated the products obtained after degradation of MG by *Photobacterium leiognathi* strain MS and in accordance with this, probable pathway was inferred. The results of impacts of different operational parameters on decolorization showed excellent ability to degrade MG dye. Destruction of MG structure led to aminobenzene derivatives and the toxicity of the degradation products was remarkably lower, indicating that the strain has a high MG detoxification potency. Enzyme analysis indicated the major involvement of laccase in the degradation of MG by *Photobacterium leiognathi* strain MS. Based on the results above, as well as the fact that this bacterium is competent to withstand both the environments (High and Low salinity), this study suggests that *Photobacterium leiognathi* strain MS is a supreme choice for the bioremediation of textile effluents in all sort of water environments.

Declarations of interest

None.

Funding

This research did not receive any specific grant from funding agencies in the public, commercial, or not-for-profit sectors.

Acknowledgement

Asif S. Tamboli is thankful to Council of Scientific & Industrial Research, New Delhi for Senior Research Fellowship (SRF) (Award number- 09/816(0042)/2018-EMR-I and ACK No-263 113307/2K17/1). DST-INSPIRE meritorious fellowship to Ms. Devashree N. Patil from DST, New Delhi, India is gratefully acknowledged.

Appendix A. Supplementary data

Supplementary data to this article can be found online at https://doi.org/10.1016/j.bcab.2019.101183.

References

Akinboro, A., Bakare, A.A., 2007. Cytotoxic and genotoxic effects of aqueous extracts of five medicinal plants on *Allium cepa Linn*. J. Ethnopharmacol. 112, 470–475. https://doi.org/10.1016/j.jep.20.

Amin, H., Arain, B.A., Amin, F., Surhio, M.A., 2013. Phytotoxicity of chromium on germination, growth and biochemical attributes of *Hibiscus esculentus* L. Am. J. Plant Sci. 4, 2431–2439. https://doi.org/10.4236/ajps.2013.412302.

An, S., Min, S., Cha, I., Choi, Y., Cho, Y., Lee, Y., 2002. Decolorization of triphenylmethane and azo dyes by *Citrobacter sp*. Biotechnol. Lett. 24, 1037–1040.

Ayed, L., Chaieb, K., Cheref, A., Bakhrouf, A., 2009. Biodegradation of triphenylmethane dye malachite green by *Sphingomonas paucimobilis*. World J. Microbiol. Biotechnol. 25, 705–711. https://doi.org/10.1007/s11274-008-9941-x.

Cha, C., Doerge, D.R., Cerniglia, C.E., 2001. Biotransformation of malachite green by the fungus *Cunninghamella elegans*. Appl. Environ. Microbiol. 67, 4358–4360. https://doi.org/10.1128/AEM.67.9.4358.

Cheriaa, J., Bakhrouf, A., 2009. Triphenylmethanes, malachite green and crystal violet dyes decolourisation by *Sphingomonas paucimobilis*. Ann. Microbiol. 59 (1), 57–61.

Chen, C.C., Lu, C.S., Chung, Y.C., Jan, J.L., 2007. UV light induced photodegradation of malachite green on TiO_2 nanoparticles. J. Hazard Mater. 141, 520–528. https://doi.org/10.1016/j.jhazmat.2006.07.011.

Chukwujekwu, J.C., Van Staden, J., 2014. Cytotoxic and genotoxic effects of water extract of *Distephanus angulifolius* on *Allium cepa* Linn. South Afr. J. Bot. 92, 147–150.

Culp, S.J., Beland, F.A., 1996. Malachite green : a toxicological review. J. American Coll. Toxicol 15, 219–238.

Daneshvar, N., Ayazloo, M., Khataee, A.R., Pourhassan, M., 2007. Biological decolorization of dye solution containing malachite green by microalgae *Cosmarium sp*. Bioresour. Technol. 98, 1176–1182. https://doi.org/10.1016/j.biortech.2006.05.025.

Deng, D., Guo, J., Zeng, G., Sun, G., Red, C., 2008. Decolorization of anthraquinone, triphenylmethane and azo dyes by a new isolated *Bacillus cereus* strain DC11. Int. Biodeterior. Biodegrad. 62, 263–269. https://doi.org/10.1016/j.ibiod.2008.01.017.

Du, L.-N., Zhao, M., Li, G., Xu, F., Chen, W., Zhao, Y., 2013. Biodegradation of malachite green by *Micrococcus sp*. strain BD15 : biodegradation pathway and enzyme analysis. Int. Biodeterior. Biodegrad. 78, 108–116. https://doi.org/10.1016/j.ibiod.2012.12.011.

Du, L.-N., Wang, S., Li, G., Wang, B., Jia, X.-M., Zhao, Y.-H., Chen, Y.-L., 2011. Biodegradation of malachite green by *Pseudomonas sp.* strain DY1 under the aerobic condition : characteristics, degradation products, enzyme analysis and phytotoxicity. Ecotoxicology 20, 438–446. https://doi.org/10.1007/s10646-011-0595-3.

Jadhav, J.P., Govindwar, S.P., 2006. Biotransformation of malachite green by *Saccharomyces cerevisiae* MTCC 463. Yeast 23, 315–323. https://doi.org/10.1002/yea.1356.

Jasinska, A., Rozalska, S., Bernat, P., Paraszkiewicz, K., Dlugonski, J., 2012. Malachite green decolorization by non-basidiomycete filamentous fungi of *Penicillium pinophilum* and *Myrothecium roridum*. Int. Biodeterior. Biodegrad. 73, 33–40. https://doi.org/10.1016/j.ibiod.2012.06.025.

Jones, J.J., Falkinham, J.O., 2003. Decolorization of malachite green and crystal violet by waterborne pathogenic mycobacteria. Am. Soc. Microbiol. 47, 2323–2326. https://doi.org/10.1128/AAC.47.7.2323.

Kagalkar, A.N., Jadhav, M.U., Bapat, V.A., Govindwar, S.P., 2011. Phytodegradation of the triphenylmethane dye malachite green mediated by cell suspension cultures of *Blumea malcolmii* hook. Bioresour. Technol. 102, 10312–10318. https://doi.org/10.1016/j.biortech.2011.08.101.

Lade, H., Kadam, A., Paul, D., Govindwar, S., 2015. Biodegradation and detoxification of

textile azo dyes by bacterial consortium under sequential microaerophilic/aerobic processes. EXCLI J. 14, 158–174. https://doi.org/10.17179/excli2014-642.

Lee, B.-S., Lee, J.-G., Shin, D.-H., Kim, E.-K., 2001. Statistical optimization of bioluminescence of *Photobacterium phosphoreum* KCTC2852. J. Biosci. Bioeng. 92, 72–76.

Lee, J.B., Kim, M., 2012. Photo-degradation of malachite green in mudfish tissues - investigation of UV-induced photo-degradation. Food Sci. Biotechnol. 21, 519–524. https://doi.org/10.1007/s10068-012-0066-5.

Oturan, M.A., Guivarch, E., Oturan, N., Sire, I., 2008. Oxidation pathways of malachite green by Fe_3^+ -catalyzed electro-fenton process. Appl. Catal., B 82, 244–254. https://doi.org/10.1016/j.apcatb.2008.01.016.

Ren, S., Guo, J., Zeng, G., Sun, G., 2006. Decolorization of triphenylmethane, azo, and anthraquinone dyes by a newly isolated *Aeromonas hydrophila* strain. Environ. Biotechnol. 72, 1316–1321. https://doi.org/10.1007/s00253-006-0418-2.

Shedbalkar, U., Jadhav, J.P., 2011. Detoxification of malachite green and textile industrial effluent by *Penicillium ochrochloron*. Biotechnol. Bioproc. Eng. 204, 196–204. https://doi.org/10.1007/s12257-010-0069-0.

Singh, A.K., Nakate, U.T., 2013. Photocatalytic properties of microwave-synthesized TiO2 and ZnO nanoparticles using malachite green dye. J. Nanopart. 7 2013. https://doi.org/10.1155/2013/310809.

Srivastava, S., Sinha, R., Roy, D., 2004. Toxicological effects of malachite green. Aquat. Toxicol. 66, 319–329. https://doi.org/10.1016/j.aquatox.2003.09.008.

Timothy, O., Idu, M., Olorunfemi, D.I., Ovuakporie-Uvo, O., 2014. Cytotoxic and genotoxic properties of leaf extract of *Icacina trichantha* Oliv. South Afr. J. Bot. 91, 71–74. https://doi.org/10.1016/j.sajb.2013.11.008.

Wang, J., Gao, F., Liu, Z., Qiao, M., Niu, X., Zhang, K., Huang, X., 2012. Pathway and molecular mechanisms for malachite green biodegradation in *Exiguobacterium sp.* MG2. PLoS One 7, e51808. https://doi.org/10.1371/journal.pone.0051808.

Wang, J., Qiao, M., Wei, K., Ding, J., Liu, Z., Zhang, K.-Q., Huang, X., 2011. Decolorizing activity of malachite green and its mechanisms involved in dye biodegradation by *Achromobacter xylosoxidans* MG1. J. Mol. Microbiol. Biotechnol. 20 (4), 220–227. https://doi.org/10.1159/000330669.

Watkins, O.C., Sharpe, M.L., Perry, N.B., Krause, K.L., 2018. New Zealand glowworm bioluminescence is produced by a firefly-like luciferase but an entirely new luciferin. Sci. Rep. 8, 1–15. https://doi.org/10.1038/s41598-018-21298-w.

Wu, J., Jung, B.-G., Kim, K.-S., Lee, Y.-C., Sung, N.-C., 2009. Isolation and characterization of *Pseudomonas otitidis* WL-13 and its capacity to decolorize triphenylmethane dyes. J. Environ. Sci. 21, 960–964. https://doi.org/10.1016/S1001-0742(08)62368-2.

Yang, J., Yang, X., Lin, Y., Ng, T.B., Lin, J., Ye, X., 2015. Laccase-catalyzed decolorization of malachite green : performance optimization and degradation mechanism. PLoS One 28, 1–14. https://doi.org/10.1371/journal.pone.0127714.